

Banner appropriate to article type will appear here in typeset article

Adjoint-based particle forcing reconstruction and uncertainty quantification

Daniel Domínguez-Vázquez¹, Qi Wang^{†1} and Gustaaf B. Jacobs¹

¹San Diego State University, 5500 Campanile Dr, San Diego, CA 92182

(Received xx; revised xx; accepted xx)

The forcing of particles in turbulent environments influences dynamical properties pertinent to many fundamental applications of particle-flow interactions. Current study explores the determination of forcing for one-way coupled passive particles, under the assumption that the ambient velocity fields are known. When measurements regarding particle locations are available but sparse, direct evaluation of the forcing is intractable. Nevertheless, the forcing for finite-size particles is determined using adjoint-based data assimilation. This inverse problem is formulated within the framework of optimization, where the cost function is defined as the difference between the measured and predicted particle locations. The gradient of the cost function, with respect to the forcing can be calculated from the adjoint dynamics. When measurements are subject to Gaussian noise, samples within the probability distribution of the forcing can be drawn using Hamiltonian Monte Carlo (HMC). The algorithm is tested in the Arnold-Beltrami-Childress (ABC) flow as well as the homogenous isotropic turbulence. Results demonstrate that the forcing can only be determined accurately for particle Reynolds number between 1 and 5, where the majority of Reynolds number history along the particle trajectory falls in.

Key words:

1. Introduction

The physics of dispersed particle fields in unsteady and turbulent flow fields is intricate. This has been and continues to be the inspiration of a significant amount of research on the modeling of particle-laden flow. While several textbooks such Crowe *et al.* (1998); Marchisio & Fox (2007); Ishii (1975) and review articles Brandt & Coletti (2022) have summarized a large number of approaches and an even larger number of models, a key issue in constructing robust and accurate computational models for the dynamic behavior of the dispersed particle fields remains the formulation of accurate particle forcing models. The current research aims at establishing the methodological framework for adjoint-based inverse modelling of the particle forcing dynamics with uncertainty quantification when sparse, noisy measurements data along the particle trajectories is available.

[†] Email address for correspondence: qwang4@sdsu.edu

Abstract must not spill onto p.2

1.1. Particle Forcing Models

The flow forcing of a single smooth spherical object in uniform flow is well-known and described analytically for low Reynolds and Mach number by the Maxey-Riley equation (Maxey & Riley 1983). Resolution requirements and the complexity of the interaction between wakes, boundary layers, turbulence and shocks, however, limit the accurate measurement and prediction for flow conditions outside of that range. At higher Reynolds numbers, for example, the flow separates, and can become unstable and the forcing depends on subtle linear and non-linear instabilities that can be sensitive to small changes in the flow conditions. For scenarios with high-Reynolds number effects, for example, simulations of explosively dispersed particle fields originating from a high-speed moving source, basic empirical forcing models have been used (Boiko *et al.* 1997; Jacobs & Don 2009; Jacobs *et al.* 2012). However, it is clear that the accuracy of such models is affected by unsteady forcing (Sen *et al.* 2018a) and unsteady carrier-phase effects (Sen *et al.* 2019). In fact, high-speed particle flow has spurred model development over the last decade (Capecelatro *et al.* 2014; Jacobs *et al.* 2012) and led to studies that determine either theoretically, experimentally or through machine learning the particle forcing of single particles affected by moving shocks (Kiselev *et al.* 2006; Ling *et al.* 2011; Parmar *et al.* 2009) and arrays of particle affected by shock diffraction (Sen *et al.* 2017; Ling *et al.* 2012; Mehta *et al.* 2016; Capecelatro *et al.* 2014; Tryggvason & Dabiri 2013; Regele *et al.* 2012, 2014).

In addition to the impact of flow conditions, a range of geometric parameters can affect the particle. For example micro- and meso-scopic, but crucial geometric imperfections and deformation of (condensed) particles' surfaces impacts on momentum and energy exchange with a carrier flow. A harmonic perturbation of cylindrical shape for example can change the dominant vorticity generation by shear to a baroclinic mechanism (Blanco-Casares & Jacobs 2022) and yield different forcing. Just these few examples show how many parameters and flow conditions can affect forcing models, and it should not be surprising that an accurate and comprehensive forcing model has eluded the community and realistically is not be feasible for all conditions.

As an alternative to understanding the effect of more flow conditions (free-stream turbulence, free-stream velocity profile, stratification etc.) or particle geometry and the formulation of even more additional and new forcing corrections, we might consider the forcing problem from an inverse perspective and resolve the limitations of modeling and experiment through inference and optimization from observational and simulated data using analytical relations and inputs and outputs of simulation and experiment. Could we, for example, infer the forcing from limited trajectory data? Or might it be possible to assume a random forcing models with a confidence interval and improve this forcing with a limited amount of high-resolution data? To this end an intelligent framework is required that systematically and robustly improves forcing models and associated macro-response protocols with a robust uncertainty quantification using limited, experimental data.

1.2. Inverse methods

The inference of particle forcing from sparse measurements can be accomplished from an inverse-problem perspective. The dependence of the measurements, either individual particle trajectory data or shape of the cloud distribution, onto the forcing law is highly nonlinear, obtained from solving the physical governing equations. In general, for such nonlinear physics-constrained inverse problems, two different classes of methods are considered in past researches. Data-based methods aim at learning massive amount of data as a distribution, often in reduced-order latent space. Methods such as Generative adversarial networks (GANs) (Hassanali *et al.* 2022; Silva *et al.* 2021a,b; Legler & Janjić 2022), Auto-encoders (Wang

et al. 2022b; Peyron *et al.* 2021; Amendola *et al.* 2020) or Long-Short-Term Memory (LSTM) (Wan & Sapsis 2018) can successfully discover the intrinsic coordinates of the data and take into account the effect of observing by evaluating the probability distribution conditioned on those observations. However, giving the efficiency and practicality of these methods, a thorough physical analysis of the results is often difficult because the foundation is not the governing equation. Model-based methods, on the other hand, initiate from the governing equation and often need to solve the adjoint equations to obtain the gradient of the cost function (Wang *et al.* 2019c). To maintain consistency with the forward solver and ensure numerical stability during optimization, discrete adjoint operator is often derived and implemented (Wang *et al.* 2019a). Furthermore, the adjoint fields by solving the adjoint equations gives clear interpretation of the physical meaning (Wang *et al.* 2022a) as the domain of dependence.

One significant benefit of data-based methods is that uncertainty quantification is straightforward under the probabilistic framework. However, for model-based methods, uncertainty quantification is often much more difficult in terms of the adjoint dynamics. For linear dynamics, Bayesian inference with uncertainty quantification can be easily performed using Gaussian Process Regression (GPR) through the aid of adjoint (Gahungu *et al.* 2022). For nonlinear dynamics, distribution of the control vector deviates from Gaussian and samples of the probability distribution can be draw from Hamiltonian Monte Carlo (HMC) using the gradient Langevin dynamics (Yang *et al.* 2021; Herrmann *et al.* 2019). A remaining hassle would be the computational cost to solve both the forward and adjoint governing equations repetitively.

To account for parametric, empirical and structural uncertainty fluctuations in forcing models, a probabilistic (stochastic), point-particle and multi-scale perspective as was taken in Jacobs & Udaykumar (2019) and Domínguez-Vázquez *et al.* (2021). Starting from known empirical models and/or surrogate forcing models from high-resolution simulations (Sen *et al.* 2018b), that account for Reynolds, Mach number and number density, and other parameters, we can describe the forcing and its dependencies within confidence intervals according to a probability density function. Stochastic dynamic models are formulated that propagate this distribution into the stochastic solutions of trajectories (Domínguez-Vázquez *et al.* 2021).

In this paper, we reconstruct forcing models using a combination of governing dynamic equations that govern the location and velocity of a particle modeled as a singular point with an unknown forcing and adjoint formulations. We develop a theoretical framework that determines forcing for one-way coupled passive particles, under the assumption that the ambient velocity fields are known.

The remainder of the paper is organized as follows: firstly we focus on point-particle and particle forcing models and derive the optimization framework based utilizing the adjoint dynamics. The forcing reconstruction is then practiced in two test cases, the Arnold–Beltrami–Childress (ABC) flow and a decaying isotropic turbulence flow.

2. Problem Formulation

Consider the motion of a single particle with trajectory $\mathbf{x}_p(t)$ and velocity $\mathbf{u}_p(t)$. The non-dimensional governing equations for the particle read

$$\frac{d\mathbf{x}_p}{dt} = \mathbf{u}_p, \quad \frac{d\mathbf{u}_p}{dt} = \frac{f}{St} (\mathbf{u} - \mathbf{u}_p), \quad (2.1)$$

where \mathbf{u} is the ambient velocity at the particle location \mathbf{x}_p . The Stokes number is defined as the ratio between the characteristic time of the flow and the particle phase, and can be

expressed in terms of the reference Reynolds of the flow as $St = Re_\infty \frac{\rho_p d_p^2}{18}$ where d_p is the non-dimensional particle diameter and ρ_p is the density ratio of the two phases. The function f is the forcing coefficient as a fix for Stokes flow. For Stokes flow, f becomes the unity function. In more general cases, the forcing term f is a function of the slip velocity, $f = f(|\mathbf{u} - \mathbf{u}_p|) = f(a)$.

The governing equation is integrated using simple forward Euler scheme, with two ambient velocity fields considered in the current study: the Arnold–Beltrami–Childress (ABC) flow and the decaying homogeneous isotropic turbulence obtained from Johns Hopkins Turbulence Database (JHTDB) (Li *et al.* 2008), computed with an in-house discontinuous Galerkin (DG) DNS solver described in Klose *et al.* (2020) and references therein, with initial conditions adopted from Jacobs *et al.* (2005).

In principle, f lives in the infinite dimensional space. In the current study, we adopted one of the most common forcing models (Boiko *et al.* 1997; Jacobs *et al.* 2012) as the ground truth,

$$f(a) = \left(1 + 0.38 \frac{Re_p}{24} + \frac{1}{6} \sqrt{Re_p}\right), \quad (2.2)$$

with the particle Reynolds number defined as $Re_p = Re_\infty a d_p$.

In computations, proper low-rank approximation of the forcing function has to be applied, and the forcing is discretized as a linear superposition of orthogonal basis functions,

$$f(a) = \sum_i \alpha_i \psi_i(a), \quad \psi_i(a) = \cos\left(i \frac{2\pi d_p Re_\infty}{2Re_{p,max}} a\right), \quad (2.3)$$

where $Re_{p,max}$ is set to be slightly more than the maximum particle Reynolds number encountered in the simulation. We denote the parameters α for dimensional reduction. The determination of f is then reduced to the determination of the parameters α .

2.1. Adjoint optimization algorithm

When sparse measurements for the particle trajectory are available, information regarding the forcing is indirect. We consider a special case, where the measurement is only available at the final time t_m . The cost function in this case can be defined as the difference between the computed and measured particle locations at t_m , namely,

$$J = \frac{1}{2} \|\mathbf{x}_m - \mathbf{x}_p(t_m)\|^2. \quad (2.4)$$

For general cases where measurements are available for several different t_m , a simple summation of the individual cost functions will be adopted and a similar procedure is still valid.

To satisfy the governing equations 2.1 in addition to minimize the cost function 2.4, we augment the cost function with the Lagrange multiplier \mathbf{x}_p^\dagger , \mathbf{u}_p^\dagger , which results in the function \mathcal{H} ,

$$\mathcal{H} = J + \int_t \left[\mathbf{x}_p^\dagger \cdot \left(\frac{d\mathbf{x}_p}{dt} - \mathbf{u}_p \right) + \mathbf{u}_p^\dagger \cdot \left(\frac{d\mathbf{u}_p}{dt} - \frac{f}{St} (\mathbf{u} - \mathbf{u}_p) \right) \right] dt. \quad (2.5)$$

If the forcing parameters α are perturbed by an amount $\delta\alpha$, the change of forcing would result in a deviation of \mathbf{x}_p and \mathbf{u}_p from its original trajectory, perturbed by the amount $\delta\mathbf{x}_p$ and $\delta\mathbf{u}_p$, respectively. In particular, the perturbation of the ambient velocity $\mathbf{u}|_{\mathbf{x}_p}$ can be obtained from

$$\delta\mathbf{u}|_{\mathbf{x}_p} = \nabla\mathbf{u}|_{\mathbf{x}_p} \cdot \delta\mathbf{x}_p. \quad (2.6)$$

In addition, the change of forcing $f(a)$ can be evaluated as,

$$\begin{aligned}\delta[f(a)] &= \delta\left[\sum_i \alpha_i \psi_i(|\mathbf{u} - \mathbf{u}_p|)\right] \\ &= \sum_i \delta\alpha_i \psi_i(|\mathbf{u} - \mathbf{u}_p|) + \frac{f'(a)}{a} \left(\nabla \mathbf{u}|_{\mathbf{x}_p} \cdot \delta \mathbf{x}_p - \delta \mathbf{u}_p\right) \cdot (\mathbf{u} - \mathbf{u}_p)\end{aligned}\quad (2.7)$$

The perturbation of the cost function can be evaluated as,

$$\begin{aligned}\delta \mathcal{H} &= \frac{\partial J}{\partial \mathbf{x}_p} \delta \mathbf{x}_p + \frac{\partial J}{\partial \mathbf{u}_p} \delta \mathbf{u}_p + \int_t \mathbf{x}_p^\dagger \cdot \left(\frac{d\delta \mathbf{x}_p}{dt} - \delta \mathbf{u}_p\right) dt \\ &+ \int_t \mathbf{u}_p^\dagger \cdot \left\{ \frac{d\delta \mathbf{u}_p}{dt} - \frac{1}{St} f(a) (\nabla \mathbf{u} \cdot \delta \mathbf{x}_p - \delta \mathbf{u}_p) - \frac{1}{St} \delta[f(a)] (\mathbf{u} - \mathbf{u}_p) \right\} dt.\end{aligned}\quad (2.8)$$

Through integration by parts, we can obtain another form,

$$\begin{aligned}\delta \mathcal{H} &= \int_t \delta \mathbf{x}_p \cdot \underbrace{\left[-\frac{d\mathbf{x}_p^\dagger}{dt} - \frac{1}{St} (\nabla \mathbf{u})^T \cdot \left[f(a) \mathbf{u}_p^\dagger + \frac{f'(a)}{a} [(\mathbf{u} - \mathbf{u}_p) \cdot \mathbf{u}_p^\dagger] (\mathbf{u} - \mathbf{u}_p) \right] + \frac{\partial J}{\partial \mathbf{x}_p} \right]}_{=0, \text{adjoint equations}} dt \\ &+ \int_t \delta \mathbf{u}_p \cdot \underbrace{\left[-\frac{d\mathbf{u}_p^\dagger}{dt} - \mathbf{x}_p^\dagger + \frac{1}{St} \left[f(a) \mathbf{u}_p^\dagger + \frac{f'(a)}{a} [(\mathbf{u} - \mathbf{u}_p) \cdot \mathbf{u}_p^\dagger] (\mathbf{u} - \mathbf{u}_p) \right] + \frac{\partial J}{\partial \mathbf{u}_p} \right]}_{=0, \text{adjoint equation}} dt \\ &- \frac{1}{St} \int_t \sum_i \delta \alpha_i \psi_i(|\mathbf{u} - \mathbf{u}_p|) \mathbf{u}_p^\dagger \cdot (\mathbf{u} - \mathbf{u}_p) dt.\end{aligned}\quad (2.9)$$

In case of the single measurement at t_m , the derivatives of the cost function are,

$$\frac{\partial J}{\partial \mathbf{x}_p} = (\mathbf{x}_p(t_m) - \mathbf{x}_m) \delta(t - t_m), \quad \frac{\partial J}{\partial \mathbf{x}_p} = \mathbf{0}. \quad (2.10)$$

in backward time axis $\tau = t_m - t$. The initial conditions of the adjoint simulations are defined as,

$$\mathbf{x}_p^\dagger = \mathbf{u}_p^\dagger = \mathbf{0}, \quad \tau = 0. \quad (2.11)$$

Although the source term of the adjoint equation, $\partial J / \partial \mathbf{x}_p$ can be taken into account in the initial condition instead, we here retain the most general form so that the adjoint equations apply to a general cost function. Also notice that the adjoint equation involves a singularity around $a = |\mathbf{u} - \mathbf{u}_p| = 0$, corresponding to the vanishing forcing when $\mathbf{u} - \mathbf{u}_p = \mathbf{0}$ in the forward equation.

By solving the adjoint equations backwards in time, we obtain the final gradients as,

$$\frac{\partial H}{\partial \alpha_i} = -\frac{1}{St} \int_t \psi_i(|\mathbf{u} - \mathbf{u}_p|) \mathbf{u}_p^\dagger \cdot (\mathbf{u} - \mathbf{u}_p) dt. \quad (2.12)$$

In the current study, the discretization of the adjoint equations are derived from summation by parts using the discretized forward equations. This approach, instead of discretizing the adjoint equations derived from integration by parts, is called the discrete adjoint (Wang *et al.* 2019b). The discrete adjoint calculates the gradient directions $\partial H / \partial \alpha$ accurately to machine zero and guarantees the convergence of the optimization algorithm.

2.2. Hamiltonian Monte Carlo

Hamiltonian Monte Carlo, which is known as a golden approach for sampling from posterior distributions, is an efficient Markov Chain Monte Carlo (MCMC) method based on the Hamiltonian dynamics. Suppose that the posterior distribution of the unknown flow parameters, α , follows the distribution,

$$p(\alpha) \sim \exp\left(-\frac{J(\alpha)}{\sigma^2}\right). \quad (2.13)$$

Given the form of the cost function J being quadratic, we are sampling from the posterior distribution of the flow state given measurements being Gaussian variables. To sample from this given posterior, HMC constructs a Hamiltonian system with a fictitious momentum variable \mathbf{r} ,

$$H(\alpha, \mathbf{r}) = \frac{J}{\sigma^2} + \frac{1}{2}\mathbf{r}^T \mathbf{M}^{-1}\mathbf{r}, \quad (2.14)$$

and we will sample from the joint distribution

$$\pi(\alpha, \mathbf{r}) \sim \exp\left(-\frac{J(\alpha)}{\sigma^2} - \frac{1}{2}\mathbf{r}^T \mathbf{M}^{-1}\mathbf{r}\right), \quad (2.15)$$

for which we ignore the part for the momentum and obtain the marginal distribution for α . The sampling is done by selecting \mathbf{r} from its Gaussian distribution and integrate equation (2.14) using symplectic algorithms such as leapfrog. In addition, Metropolis-Hastings step is incorporated to enhance the efficiency of the sampling (Chib & Greenberg 1995). Algorithmically, it enables the original adjoint-based gradient descend algorithm (Wang *et al.* 2019*d,b*) to extend to a probabilistic framework by adding randomness.

The overall procedure of HMC is shown in algorithm 1. The gradient of the cost function, ∇_{α} is evaluated from adjoint simulations and using equation (2.12). The computational cost for solving the adjoint equation is comparable to solving the forward problem and does not depend on the number of unknown parameters, e.g. the size of α . In the current study, the parameters for HMC are set considering the efficiency for both the number of equation-solving and convergence behavior of the Monte Carlo sampling.

3. Applications

3.1. One-parameter estimation in the ABC flow

We first consider the Arnold–Beltrami–Childress (ABC) flow (Jeffreys 1928), a three-dimensional steady analytical solution of the Euler equation, with the constants of the carrier flow field chosen as $A = \sqrt{3}$, $B = \sqrt{2}$ and $C = 1$. The flow field is shown in figure 1, with particle originated at rest from $\mathbf{x}_{p,0} = (\pi, \pi, \pi)^T$ with different Stokes numbers $St = \{1, 2, 5, 10\}$. As a demonstration of the data assimilation and adjoint-based uncertainty quantification, we focus on a simple one-parameter reconstruction, where the forcing function is assumed to be,

$$f(a) = \alpha\psi(a), \quad \psi(a) = \left(1 + 0.38\frac{Re_p(a)}{24} + \frac{1}{6}\sqrt{Re_p(a)}\right), \quad (3.1)$$

where α is the only unknown parameter. Here we fix the Stokes number $St = 1$ while bringing the readers to the equivalent effect between changing α and changing St .

For α fluctuating in a range $0.95 \leq \alpha \leq 1.05$, the trajectory of the particle, \mathbf{x}_p varies slightly, as shown in figure 1(a) in the upper panel. As the true value of α is $\alpha_T = 1$, the other perturbed values of α lead to mismatched observations at the time $t = t_m = 8$. As

Algorithm 1: Hamiltonian Monte Carlo

Input: A starting parameter α_0 and step size δt

Output: Samples of the parameter α_i drawn from its posterior distribution.

for $i \leftarrow 1$ **to** N **do**

 Draw \mathbf{r}_{i-1} from $\mathcal{N}(0, \mathbf{M})$

$(\tilde{\alpha}_0, \tilde{\mathbf{r}}_0) \leftarrow (\alpha_{i-1}, \mathbf{r}_{i-1})$

for $j \leftarrow 0$ **to** $L - 1$ **do**

$\tilde{\mathbf{r}}_j \leftarrow \tilde{\mathbf{r}}_j - \frac{1}{2}\delta t \nabla_{\alpha} \mathcal{J}(\tilde{\alpha}_j)$

$\tilde{\alpha}_{j+1} \leftarrow \tilde{\alpha}_j + \delta t \mathbf{M}^{-1} \tilde{\mathbf{r}}_j$

$\tilde{\mathbf{r}}_j \leftarrow \tilde{\mathbf{r}}_{j+1} - \frac{1}{2}\delta t \nabla_{\alpha} \mathcal{J}(\tilde{\alpha}_{j+1})$

 Metropolis-Hasting algorithm:

$p \leftarrow \min\{1, \exp(-H(\tilde{\alpha}_L, \tilde{\mathbf{r}}_L) + H(\alpha_{i-1}, \mathbf{r}_{i-1}))\}$

 Draw β from uniform distribution in $[0, 1]$

if $\beta \leq p$ **then**

$\alpha_i \leftarrow \tilde{\alpha}_L$

else

$\alpha_i \leftarrow \alpha_{i-1}$

Use α_i as samples of α

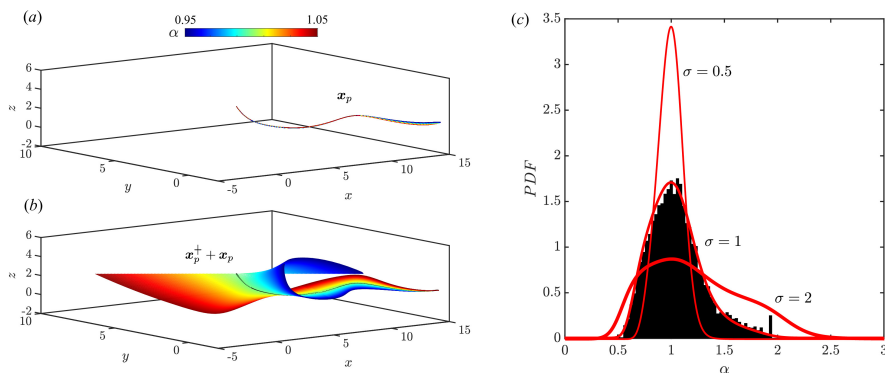


Figure 1: (a): The particle trajectories from $t = 0$ to $t = t_m = 8$ for different values of α , while the true value is $\alpha_t = 1$. Increasing values of α from 0.95 to 1.05 are marked by different colors. (b): The adjoint particle trajectories $\mathbf{x}_p^\dagger + \mathbf{x}_p$ given the true measurement $\mathbf{x}_p(t = t_m)$. Increasing Stokes number are marked with the same color map as (a). (c): When the measurement data $\mathbf{x}_p(t = t_m)$ has Gaussian error with standard deviation σ , the posterior probability distribution of the value α is estimated both theoretically and by using HMC. Red lines marks the theoretical results with different level of Gaussian noise $\sigma = \{0.5, 1, 2\}$ while the histogram shows the result from HMC with $\sigma = 1$.

illustrated in equations (2.9) and (2.10), the initial position of the adjoint particles are given by the mismatch of the observation, $\mathbf{x}_p^\dagger(t_m) = \mathbf{x}_m - \mathbf{x}_p(t_m)$, therefore, the trajectory $\mathbf{x}_p^\dagger + \mathbf{x}_p$ originates all from the same location \mathbf{x}_m at the measurement time t_m , and travels backwards in time, forming a collection of adjoint particle tracers shown in figure 1(a) on the bottom panel. We here stress the important properties between the forward and adjoint trajectories: nearby particles separates according to the same Lyapunov exponent: a conclusion directly derived from the transposed dynamics of the adjoint (Wang *et al.* 2022a).

The gradient of the cost function with respect to the parameter α is then given by the

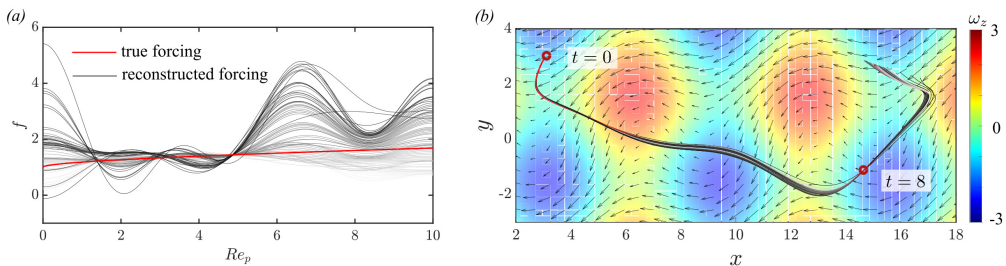


Figure 2: (a) Collection of reconstructed forcing starting from different initial guesses $f = \alpha_0 \in [0, 4]$, darker color marks higher values of α_0 in the initial guess. Red line marks the true forcing. (b) Top view of the collection of reconstructed particle traces. The locations of the particle at the initial $t = 0$ and observation time $t = 8$ are known and marked by the red circle. Colors of the particle traces correspond to the ones in (a). Colored contours show the vorticity ω_z of the background flow field at $z = 0$.

forward and adjoint particle velocities, as shown in equation (2.12). For different tolerance of observation error σ , the posterior distribution of the parameter α can be estimated through the HMC algorithm described in section 2.2. For this simple example with only one parameter, the PDF is also evaluated either through a direct mapping between α and $\mathbf{x}_p(t_m)$ as a validation for the HMC algorithm. Both results are shown in figure 1(b). Results with HMC with $\sigma = 1$ shows good agreement with direct mapping.

Results for larger value of σ show increasing level of non-linearity: since the observation error follows a Gaussian distribution, the posterior distribution for the parameter would be perfectly Gaussian if the dynamic system is linear, which is the case for small σ ; the distribution would deviate from Gaussian for larger σ .

3.2. Forcing reconstruction in the ABC flow

As the next step, we consider the more general case where the forcing function is parametrized by a few Fourier modes, as illustrated in equation (2.3). In the application of ABC flow, where Re_p is below 10, a total number of seven Fourier modes is enough to efficiently represent the shape in (2.2). The particle is initialized at location $x_p = y_p = z_p = 2\pi$ at rest. The Reference Reynolds number is $Re_\infty = 250$, the Stokes number is unity $St = 1$, the particle density ratio is $\rho_p = 500$ and the non-dimensional particle diameter $d_p = 0.012$. We assume that the initial location of the particle at rest is known, and the observations of the three coordinates of the particle location is available at time $t = 8$. We choose the observation of particle position at the non-dimensional time of eight Stokes time units so that the particle trajectory is dominated by an inertial response to the changes in the flow field.

Using the gradient of the cost function, following equation (2.12), we adopted the Quasi-Newton iterative algorithm to reconstruct the forcing parameters. The initial guess is a constant forcing $f = \alpha_0$, i.e., $\alpha_1 = \alpha_2 = \dots = \alpha_6 = 0$. We start from initial guesses with α_0 ranging from 0 to 4 and arrive at different solution of the forcing that drives the cost function sufficiently small, namely $J < 10^{-6}$. Results of various reconstructed forcing functions are plotted in figure 2(a) in grey colors, darker color represents larger α_0 in the initial guess and red line marks the true forcing function. The collection of reconstructed forcing demonstrates the ill-posedness of the problem, where infinite number of possible solutions exist. However, the particle trajectories from the reconstructed forcing are plotted in figure 2(b) follow only slightly different paths that coincide at $t = 8$ before they further deviate. This also implies that even with large range of function f , the form of the forcing can only permit a limited region of arrival for the particle.

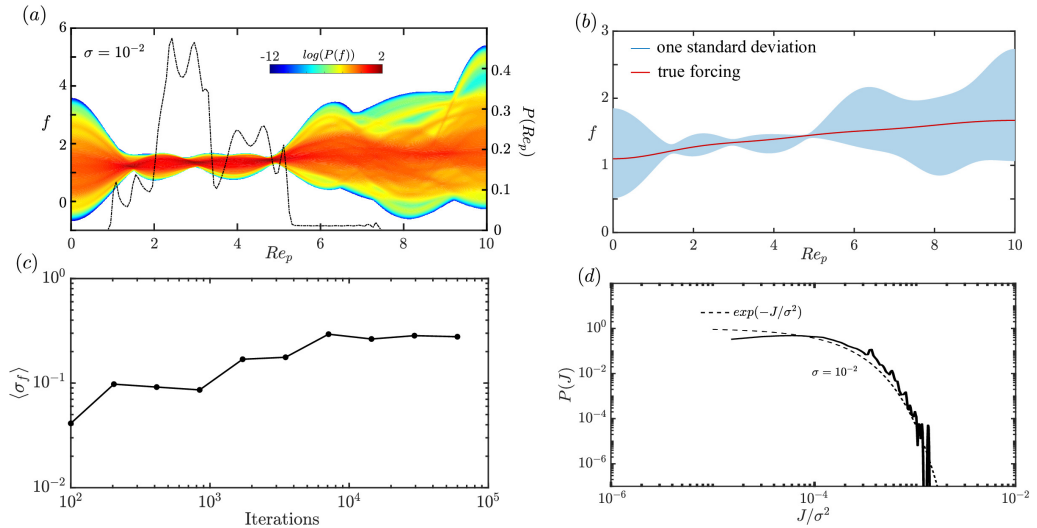


Figure 3: (a): Logarithmic of the Probability Density Function (PDF) of the forcing f during HMC sampling. The true forcing function is marked by the black line. (b) Statistics of the PDF from forcing estimation are plotted. Dashed lines represent the mean (expected values) of the forcing, while the shaded region marks forcing function within one standard deviation. The true forcing is shown by the red solid line. (c) Growth of the averaged standard deviation of the forcing distribution as more iterations are performed. (d) Probability distribution of the cost function during HMC after the burn-in period. For different level of observation uncertainty σ , the theoretical results are also shown in dashed lines.

To further quantify the uncertainty of the forcing function f , the HMC algorithm is adopted. The noise level σ is the key to the efficiency of the algorithm. A noise level that is too large would result in unconstrained forcing function with unreasonable range. On the other hand, a noise level that is too small would cause large curvature in the landscape of the cost function and cause difficulty for the sampling algorithm. With the noise level $\sigma = 0.01$, the posterior distribution for the coefficients α_i of these modes is evaluated using HMC and shown in figure 3.

In order to obtain a reasonable starting point for the HMC algorithm, we start from the true forcing parameters. In real practice when the true forcing is unknown, this could be replaced by performing a few L-BFGS iterations to update the forcing coefficients from the initial guess until we reach the desired level of tolerance. This procedure, in lieu of the traditional burn-in period, is more efficient in term to get near the true solution and serves as a fair starting point for HMC algorithm.

The posterior probability distribution of the forcing is plotted as colored contours in figure 3(a). The mean and standard deviation of the reconstructed forcing are plotted in figure 3(b). The forcing reconstruction is much more accurate in the range $1 < Re_p < 5$ than at other particle Reynolds numbers. Compared with the history of Re_p plotted in the background of figure 3(a), it is apparent that the Re_p with low uncertainty of the forcing coincide with the high probability of occurrence along the trajectories.

The distribution of the cost function during the HMC sampling is plotted in figure 3(d), where the dashed lines marks the theoretical results of $P(J) \sim \exp(-J/\sigma^2)$. The mismatch between the HMC and the theoretical prediction is due to the difficulty of sampling near the optimal parameters for high-dimensional problems due to low volume fraction interior of the typical set (Betancourt 2017).

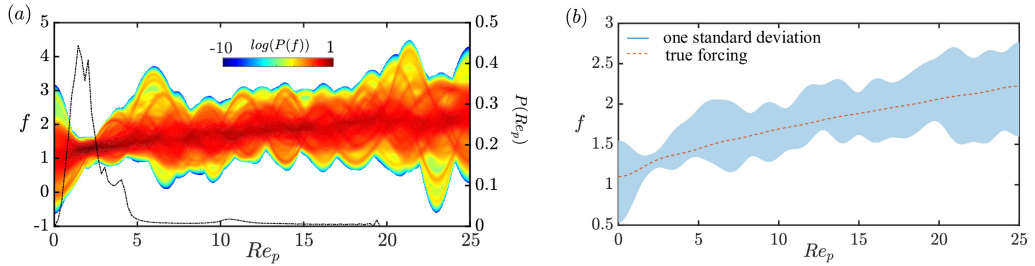


Figure 4: (a): Logarithmic of the Probability Density Function (PDF) of the forcing f reconstructed using HMC. The true forcing function is marked by the black line. (b) Statistics of the PDF from forcing estimation are plotted. Dashed lines represent the mean (expected values) of the forcing, while the shaded region marks forcing function within one standard deviation. The true forcing is shown by the red solid line. Darker colors represent less uncertainty in the observation. (c) Probability distribution of the cost function during HMC after the burn-in period. For different level of observation uncertainty σ , the theoretical results are also shown in dashed lines.

3.3. Homogeneous Isotropic Turbulence

The algorithm is also tested in three-dimensional homogeneous isotropic turbulence in a cubic domain $\Omega = [0, 2\pi] \times [0, 2\pi] \times [0, 2\pi]$. The flow fields are obtained with an in-house discontinuous Galerkin compressible DNS solver (Klose *et al.* (2020) and references therein). For the definition of the initial condition of the flow field we adopted the one used in Jacobs *et al.* (2005); Domínguez-Vázquez *et al.* (2022). The particle is initialized at location $(x_p, y_p, z_p)^\top = (\pi, \pi, 2\pi/3)^\top$ with velocity $(u_p, v_p, w_p)^\top = (0, 0, 1.5)^\top$. The Reference Reynolds number is $Re_\infty = 2,357$, the Stokes number is unity $St = 1$, the particle density ratio is $\rho_p = 250$ and the non-dimensional particle diameter $d_p = 0.0055$. The observation time here is selected to be $t = 6$, where the particle travel for six Stokes time units being the time scales of changes in the flow on the same order than those on the particle phase ($St = 1$).

The results of uncertainty quantification using 15 Fourier modes are shown in figure 4. The uncertainty of the forcing function f is the smallest for the Re_p with the most occurrence along the particle trajectory. This result is very similar to that in the ABC flow. The underlying reason is that as the particle move faster than the ambient fluid, the momentum effect becomes more and more important. For large Re_p , inertia plays a vital role and the effect of forcing become nearly negligible, rendering the determination for large Re_p much more challenging. The probability of occurrence for different Reynolds number, $P(Re_p)$ along the trajectories during the HMC sampling are also plotted in figure 3(a).

4. Conclusion

A data assimilation framework is established, to estimate the forcing of particles as a function of the relative velocity $a = |\mathbf{u}_p - \mathbf{u}|$ based on sparse, noisy measurements of the arrival location of the particle. The optimization framework relies on the adjoint dynamics of the particles, which yields the same Lyapunov exponent as the forward dynamics. Furthermore, a Hamiltonian Markov Chain is adopted for uncertainty quantification of the forcing, when measurements are subject to Gaussian noise.

The algorithm is demonstrated in ABC flow and isotropic turbulence with the Stokes number of unity. The algorithm can efficiently identifies forcing functions to accurately guide particles to the observed arrival locations. The uncertainty quantification from HMC demonstrates the ill-posedness of the problem when observations has noise. The accuracy

of the forcing depends on the history of particle Reynolds number along the trajectory. In both flows, the forcing for $1 < Re_p < 5$ can be more accurately determined than other Reynolds numbers.

The current study is the first step for data assimilation in particle forcing determination using the adjoint particle dynamics and could lead to better understanding of kinematics for particle-laden flows from experimental data, and advance the data-based development for reduced-order model for particle-flow interactions. Possible future research includes extending the framework to multiple particles with and without labels, and incorporating the hydrodynamic memory.

REFERENCES

- AMENDOLA, MADDALENA, ARCUCCI, ROSSELLA, MOTTET, LAETITIA, CASAS, CESAR QUILODRAN, FAN, SHIWEI, PAIN, CHRISTOPHER, LINDEN, PAUL & GUO, YI-KE 2020 Data assimilation in the latent space of a neural network. *arXiv preprint arXiv:2012.12056* .
- BETANCOURT, MICHAEL 2017 A conceptual introduction to hamiltonian monte carlo. *arXiv preprint arXiv:1701.02434* .
- BLANCO-CASARES, A. & JACOBS, G. B. 2022 Wall roughness effects on the supersonic flow over a circular cylinder. *Shock Waves* pp. 1–21.
- BOIKO, VM, KISELEV, VP, KISELEV, SP, POPYRIN, AN, POPLAVSKY, SV & FOMIN, VM 1997 Shock wave interaction with a cloud of particles. *Shock Waves* **7** (5), 275–285.
- BRANDT, LUCA & COLETTI, FILIPPO 2022 Particle-laden turbulence: Progress and perspectives. *Annual Review of Fluid Mechanics* **54**, 159–189.
- CAPECELATRO, JESSE, DESJARDINS, OLIVIER & FOX, RODNEY O 2014 Numerical study of collisional particle dynamics in cluster-induced turbulence. *Journal of Fluid Mechanics* **747**.
- CHIB, SIDDHARTHA & GREENBERG, EDWARD 1995 Understanding the metropolis-hastings algorithm. *The american statistician* **49** (4), 327–335.
- CROWE, C. T., SOMMERFELD, M. & TSUJI, Y. 1998 *Multiphase Flows with Droplets and Particles*. Boca Raton, FL: CRC Press LLC.
- DOMÍNGUEZ-VÁZQUEZ, DANIEL, JACOBS, GUSTAAF B & TARTAKOVSKY, DANIEL M 2021 Lagrangian models of particle-laden flows with stochastic forcing: Monte carlo, moment equations, and method of distributions analyses. *Physics of Fluids* **33** (3), 033326.
- DOMÍNGUEZ-VÁZQUEZ, D., KLOSE, B. F. & JACOBS, G. B. 2022 Closed SPARSE—a predictive particle cloud tracer. *arXiv preprint arXiv:2206.01528* .
- GAHUNGU, PATERNE, LANYON, CHRISTOPHER W, ALVAREZ, MAURICIO A, BAINOMUGISHA, ENGINEER, SMITH, MICHAEL & WILKINSON, RICHARD D 2022 Adjoint-aided inference of gaussian process driven differential equations. *arXiv preprint arXiv:2202.04589* .
- HASSANALY, MALIK, GLAWS, ANDREW, STENGEL, KAREN & KING, RYAN N 2022 Adversarial sampling of unknown and high-dimensional conditional distributions. *Journal of Computational Physics* **450**, 110853.
- HERRMANN, FELIX J, SIAHKOHI, ALI & RIZZUTI, GABRIO 2019 Learned imaging with constraints and uncertainty quantification. *arXiv preprint arXiv:1909.06473* .
- ISHII, M. 1975 *Thermo-Fluid Dynamic Theory of Two-phase Flow*. France: Eyrolles.
- JACOBS, GB, DON, WS & DITTMANN, T 2012 High-order resolution eulerian-lagrangian simulations of particle dispersion in the accelerated flow behind a moving shock. *Theoretical and Computational Fluid Dynamics* **26** (1), 37–50.
- JACOBS, GUSTAAF B & DON, WAI-SUN 2009 A high-order weno-z finite difference based particle-source-in-cell method for computation of particle-laden flows with shocks. *Journal of Computational Physics* **228** (5), 1365–1379.
- JACOBS, G. B., KOPRIVA, D. A. & MASHAYEK, F. 2005 Validation study of a multidomain spectral code for simulation of turbulent flows. *AIAA journal* **43** (6), 1256–1264.
- JACOBS, G. B. & UDAYKUMAR, H. S. 2019 Uncertainty quantification in Eulerian-Lagrangian simulations of (point-) particle-laden flows with data-driven and empirical forcing models. *International Journal of Multiphase Flow* **121**, 103114.
- JEFFREYS, HAROLD 1928 Some cases of instability in fluid motion. *Proceedings of the Royal Society of*

- London. Series A, Containing Papers of a Mathematical and Physical Character* **118** (779), 195–208.
- KISELEV, V.P., KISELEV, S.P. & VOROZHTSOV, E.V. 2006 Interaction of shock wave a particle cloud of finite size. *Shock Waves* **16**, 53–64.
- KLOSE, B. F., JACOBS, G. B. & KOPRIVA, D. A. 2020 Assessing standard and kinetic energy conserving volume fluxes in discontinuous Galerkin formulations for marginally resolved Navier-Stokes flows. *Computers & Fluids* **205**, 104557.
- LEGLER, STEFANIE & JANJIĆ, TIJANA 2022 Combining data assimilation and machine learning to estimate parameters of a convective-scale model. *Quarterly Journal of the Royal Meteorological Society* **148** (743), 860–874.
- LI, YI, PERLMAN, ERIC, WAN, MINPING, YANG, YUNKE, MENEVEAU, CHARLES, BURNS, RANDAL, CHEN, SHIYI, SZALAY, ALEXANDER & EYINK, GREGORY 2008 A public turbulence database cluster and applications to study lagrangian evolution of velocity increments in turbulence. *Journal of Turbulence* (9), N31.
- LING, Y, HASELBACHER, A & BALACHANDAR, S 2011 Importance of unsteady contributions to force and heating for particles in compressible flows: Part 1: Modeling and analysis for shock–particle interaction. *International Journal of Multiphase Flow* **37** (9), 1026–1044.
- LING, Y, WAGNER, JL, BERESH, SJ, KEARNEY, SP & BALACHANDAR, S 2012 Interaction of a planar shock wave with a dense particle curtain: Modeling and experiments. *Physics of Fluids* **24** (11), 113301.
- MARCHISIO, DANIELE L & FOX, RODNEY O 2007 *Multiphase reacting flows: modelling and simulation*, , vol. 492. Springer.
- MAXEY, MARTIN R & RILEY, JAMES J 1983 Equation of motion for a small rigid sphere in a nonuniform flow. *The Physics of Fluids* **26** (4), 883–889.
- MEHTA, Y, NEAL, C, JACKSON, TL, BALACHANDAR, S & THAKUR, S 2016 Shock interaction with three-dimensional face centered cubic array of particles. *Physical Review Fluids* **1** (5), 054202.
- PARMAR, M, HASELBACHER, A & BALACHANDAR, S 2009 Modeling of the unsteady force for shock–particle interaction. *Shock Waves* **19** (4), 317–329.
- PEYRON, MATHIS, FILLION, ANTHONY, GÜROL, SELIME, MARCHAIS, VICTOR, GRATTON, SERGE, BOUDIER, PIERRE & GORET, GAEL 2021 Latent space data assimilation by using deep learning. *Quarterly Journal of the Royal Meteorological Society* **147** (740), 3759–3777.
- REGELE, JONATHAN, RABINOVITCH, JASON, COLONIUS, TIM & BLANQUART, GUILLAUME 2012 Numerical modeling and analysis of early shock wave interactions with a dense particle cloud. In *42nd AIAA Fluid Dynamics Conference and Exhibit*, p. 3161.
- REGELE, JD, RABINOVITCH, J, COLONIUS, T & BLANQUART, G 2014 Unsteady effects in dense, high speed, particle laden flows. *International Journal of Multiphase Flow* **61**, 1–13.
- SEN, O, GAUL, NJ, DAVIS, S, CHOI, KK, JACOBS, G & UDAYKUMAR, HS 2018a Role of pseudo-turbulent stresses in shocked particle clouds and construction of surrogate models for closure. *Shock Waves* **28** (3), 579–597.
- SEN, OISHIK, GAUL, NICHOLAS J, CHOI, KK, JACOBS, GUSTAAF & UDAYKUMAR, HS 2017 Evaluation of kriging based surrogate models constructed from mesoscale computations of shock interaction with particles. *Journal of Computational Physics* **336**, 235–260.
- SEN, O., GAUL, N. J., CHOI, K. K., JACOBS, G. B. & UDAYKUMAR, H. S. 2018b Evaluation of multifidelity surrogate modeling techniques to construct closure laws for drag in shock–particle interactions. *Journal of Computational Physics* **371**, 434–451.
- SEN, OISHIK, TAVERNIERS, SOREN, DAS, PRATIK, JACOBS, GUSTAAF & UDAYKUMAR, HS 2019 Machine-learning based multi-scale model for shock-particle interactions. *Bulletin of the American Physical Society* **64**.
- SILVA, VINICIUS LS, HEANEY, CLAIRE E, LI, YAQI & PAIN, CHRISTOPHER C 2021a Data assimilation predictive gan (da-predgan): applied to determine the spread of covid-19. *arXiv preprint arXiv:2105.07729* .
- SILVA, VINICIUS LS, HEANEY, CLAIRE E & PAIN, CHRISTOPHER C 2021b Gan for time series prediction, data assimilation and uncertainty quantification. *arXiv preprint arXiv:2105.13859* .
- TRYGGVASON, GRETAR & DABIRI, SADEGH 2013 Direct numerical simulation of shock propagation in bubbly liquids. In *Bubble Dynamics and Shock Waves*, pp. 177–201. Springer.
- WAN, ZHONG YI & SAPSIS, THEMISTOKLIS P 2018 Machine learning the kinematics of spherical particles in fluid flows. *Journal of Fluid Mechanics* **857**.
- WANG, MENGZE, WANG, QI & ZAKI, TAMER A 2019a Discrete adjoint of fractional-step incompressible navier-stokes solver in curvilinear coordinates and application to data assimilation. *Journal of Computational Physics* **396**, 427–450.

- WANG, MENGZE, WANG, QI & ZAKI, TAMER A. 2019*b* Discrete adjoint of fractional-step incompressible navier-stokes solver in curvilinear coordinates and application to data assimilation. *Journal of Computational Physics* **396**, 427–450.
- WANG, QI, HASEGAWA, YOSUKE & ZAKI, TAMER A 2019*c* Spatial reconstruction of steady scalar sources from remote measurements in turbulent flow. *Journal of Fluid Mechanics* **870**, 316–352.
- WANG, QI, HASEGAWA, YOSUKE & ZAKI, TAMER A. 2019*d* Spatial reconstruction of steady scalar sources from remote measurements in turbulent flow. *Journal of Fluid Mechanics* **870**, 316–352.
- WANG, QI, WANG, MENGZE & ZAKI, TAMER A. 2022*a* What is observable from wall data in turbulent channel flow? *Journal of Fluid Mechanics* **941**, A48.
- WANG, YUEYA, SHI, XIAOMING, LEI, LILI & FUNG, JIMMY CHI-HUNG 2022*b* Deep learning augmented data assimilation: Reconstructing missing information with convolutional autoencoders. *Monthly Weather Review* .
- YANG, LIU, MENG, XUHUI & KARNIADAKIS, GEORGE EM 2021 B-pinns: Bayesian physics-informed neural networks for forward and inverse pde problems with noisy data. *Journal of Computational Physics* **425**, 109913.